Fragment-Shell Influences in Nuclear Fission*

Ulrich Mosel†
Oak Ridge National Laboratory, Oak Ridge, Tennessee 37830
and The University of Tennessee, Department of Physics and Astronomy, Knoxville, Tennessee 37916

and

H. W. Schmitt
Oak Ridge National Laboratory, Oak Ridge, Tennessee 37830
(Received 6 July 1971)

Potential-energy surfaces and shell-correction-energy surfaces for nuclei in the $A \simeq 200$ region and for actinide ($A \gtrsim 230$) have been calculated in the improved two-center model. These surfaces are shown in a two-dimensional representation as a function of the elongation and the constriction of the nuclear shape. Both the ground-state shell corrections and the fission barriers in the $A \cong 200$ region agree well with experiment. It is found that the saddle-point position in this region is shifted significantly towards smaller deformations compared with the liquid-drop-model prediction, this shift arising from a very pronounced valley in the shell-correction surface at the position of the liquid-drop-model saddle point. The implications of this finding for a nuclear mass formula and for the application of the liquid-drop model to fission of these nuclei are discussed. In both mass regions ($A \cong 200$ and $A \gtrsim 230$) the shell corrections alone show pronounced structure which changes slowly with mass number. At small deformations, up to the region of the second maximum in the potential, this structure is determined by the compound-nucleus shell structure. At larger deformations this structure is shown to arise from the shell structure of the nascent fragments, thus establishing the importance of fragment shells early in the fission process for the entire mass range $A \gtrsim 200$. As a consequence of these studies the regions of validity for the liquid-drop model in describing nuclear fission are explained. Finally, it is shown that the recently observed symmetry in the mass distribution of ^{257}Fm is due to the approach to the nucleus ^{264}Fm, which can split symmetrically into the two energetically strongly favored ^{132}Sn nuclei.

I. INTRODUCTION

The development of phenomenological methods for the calculation of shell corrections to the liquid-drop-model (LDM) potential-energy surfaces (PES's) in recent years has led to a revival of interest in fission theory. A number of calculations of PES's have been performed in the last few years with the aim of exploring their features for heavy nuclei.[1] These calculations, based on the Strutinsky prescription[2] for the calculation of shell corrections from deformed single-particle models, have been carried out using mainly an extension of the Nilsson model to higher multipole deformations, and have been relatively successful in their prediction of barrier heights in heavy elements and of shape isomeric states. One of the most interesting results has been the instability of the second barrier against asymmetric deformations.[3]

The experimental results on nuclear fission – e.g., the fragment-mass and kinetic-energy distributions and fragment excitation energies – seem to indicate that the fragment shells have an important influence on the fission process in heavy elements (see, e.g., Figs. 1 and 2 of Schmitt[4]). However, because of the particular types of single-particle models (i.e., one-center deformed potentials) used in the majority of calculations previously reported,[1-3] it has not been possible to take these fragment-shell effects quantitatively into account. Thus, for instance, the instability of the second barrier has been discussed by Gustafson, Möller, and Nilsson[5] in terms of properties of a specific Nilsson level. Although correct, this explanation does not especially help in understanding the general features of the process. It is therefore desirable to do calculations which are able to connect this result with the fragment-shell properties and thereby to determine to what extent the observed properties of nuclear fission are determined predominantly by the structure of the fissioning nucleus, or by that of the fragment nuclei – i.e., at what stage specific fragment-structure effects become important.

A nuclear model, the two-center shell model, has been developed recently and is well suited for the investigation of this problem.[6,7] It is able to describe the fragment shells on the same basis as the shells of the fissioning nucleus and to describe the complete transition between them. First calculations of the PES in this model have been published and have indicated that the fragment-shell

influence is already important in early stages of the fission process.[7]

In this paper we shall report calculations in the two-center shell model with more realistic angular-momentum-dependent terms. Fission barriers in the lighter elements ($A \approx 200$) are calculated here for the first time and are compared both with experimental results and with LDM predictions. We will also specifically analyze the shell corrections as a function of the constriction and elongation of the nucleus and show their connection with the fragment-shell structures by comparison with an independent fragment model, both in the region around mass $A \simeq 200$ and in actinide ($A \gtrsim 230$) nuclei. Present calculations are still limited to reflection symmetric configurations. The results, however, can be used directly to understand the relative success of the LDM in the description of nuclear fission in the lighter elements and its failure in the heavy-element region. The discussion of the PES in the Fm isotopes, where even in symmetric fission the doubly magic nucleus ^{132}Sn can be formed, particularly adds to the understanding of this latter question. The very recent results[8] showing increased symmetric yields in the mass distributions for the fission of Fm isotopes when going to higher mass number provide direct evidence of fragment-shell influences as described here.

II. TWO-CENTER MODEL

The Hamiltonian of our model is given by

$$H = T + \tfrac{1}{2}m\omega_\rho{}^2\rho^2 + \tfrac{1}{2}m\omega_z{}^2(|z| - z_0)^2 + V_{\rm corr} + V(\vec{l}, \vec{s}), \tag{1}$$

where $V(\vec{l}, \vec{s})$ is defined as a direct generalization of the Nilsson model:

$$V(\vec{l}, \vec{s}) = \begin{cases} C(z_0)\vec{l}_1 \cdot \vec{s} + D(z_0)[\vec{l}_1{}^2 - \tfrac{1}{2}N(N+3)] & z > 0 \\ C(z_0)\vec{l}_2 \cdot \vec{s} + D(z_0)[\vec{l}_2{}^2 - \tfrac{1}{2}N(N+3)] & z < 0\,. \end{cases} \tag{2}$$

Here $\vec{l}_1$ and $\vec{l}_2$ are the pseudoangular momenta with respect to the two centers at $z = z_0$ and $z = -z_0$, respectively. The operators $\vec{l}_1$ and $\vec{l}_2$ are defined in the stretched coordinate basis as defined by Nilsson.[9] Only for $\omega_\rho = \omega_z$ and $z_0 = 0$ are they identical with the exact angular-momentum operators. This change compared with Ref. 7 has been made because it was preferable to reproduce exactly the Nilsson model for $z_0 = 0$, thus avoiding the necessity of a redetermination of the parameters C and D. Also, the stretched representation is seen to be more realistic for deformed shapes, especially for the $\vec{l}^2$ term, when one recalls that the original purpose of this term is to compromise between the harmonic oscillator and the more realistic finite depth potentials. The stretched representation also gives better convergence properties at large deformations. In detail these operators are then given by

$$l_{ix} = -i\left(\eta\frac{\partial}{\partial\zeta_i} - \zeta_i\frac{\partial}{\partial\eta}\right) \tag{3}$$

and cyclic permutation for the other components. The stretched coordinates are given by

$$\xi = \left(\frac{m\omega_\rho}{\hbar}\right)^{1/2} x, \quad \eta = \left(\frac{m\omega_\rho}{\hbar}\right)^{1/2} y, \quad \zeta = \left(\frac{m\omega_z}{\hbar}\right)^{1/2} z; \tag{4}$$

with $\zeta_i = \zeta(z) - \zeta(\pm z_0)$, for $i = 1, 2$.

The single-particle parameters C and D depend on the half center separation z_0 in the same way as discussed in Ref. 7. They are interpolated between the values for the actinides and the Pb region on the one hand[1] and the mass region around $A \approx 100$ on the other hand.[10] The connection between them and the single-particle parameters κ and μ is, as usual,

$$C = -2\hbar\omega_0^0\kappa; \quad D = \tfrac{1}{2}C\mu\,.$$

The values for κ and μ which have been used in the calculations are listed in Table I. For $\hbar\omega_0^0$ we have used the value $\hbar\omega_0^0 = 41A^{-1/3}$ MeV.

The term $V_{\rm corr}$ in Eq. (1) is necessary for a smoothing of the potential at $z = 0$ and for the description of a smooth neck in the potential and is the same as the one used in Ref. 7:

$$V_{\rm corr} = -\frac{m}{2}\omega_z{}^2\frac{1}{2z_0{}^2}(|z| - z_0)^4\theta(z_0 - |z|)\,, \tag{5}$$

where θ is a step function [$\theta(x) = 0$ for $x < 0$, $\theta(x) = 1$ for $x > 0$].

For all further details of the Hamiltonian we refer the reader to Ref. 7 and for the mathematical details of the solution to Ref. 6. The general method is first to diagonalize the double-oscillator part of Eq. (1) by a simple matching procedure, and then to use these wave functions as a basis for the diagonalization of $V_{\rm corr}$ and $V(\vec{l}, \vec{s})$.

TABLE I. The table lists the single-particle parameters κ and μ for protons and neutrons for the two compound-nucleus regions discussed in the text and for the fragment region. They are, except for very small changes, taken from Nilsson *et al.* (Ref. 1) for the two compound-nucleus regions and from Arseniev, Sobiczewski, and Soloviev (Ref. 10) for the fragment region.

	Protons		Neutrons	
Mass region	κ	μ	κ	μ
$100 \le A \le 136$	0.0688	0.558	0.0638	0.491
$200 \le A \le 212$	0.0610	0.626	0.0636	0.370
$226 \le A \le 272$	0.0580	0.645	0.0635	0.330

After this diagonalization the total PES,

$$E = E_{\mathrm{LDM}} + E_p + \delta U, \tag{6}$$

can be easily calculated. Only the diagonal matrix elements of the pairing interaction are assumed to be contained in the LDM; no further renormalization of the pairing energy has been made. The LDM energy is computed with the Myers-Swiatecki mass formula parameters.[11] The shape of the liquid drop is given by the equipotential surface that coincides with the nuclear radius for the spherical shape:

$$\rho(z) = a\left[1 - \frac{(|z| - z_0)^2}{c^2}\left(1 - \frac{1}{2z_0^2}(|z| - z_0)^2\theta(z_0 - |z|)\right)\right]^{1/2}. \tag{7}$$

The shell-correction energy δU is obtained from the Strutinsky prescription[2] with a correction polynomial of sixth order and a smearing width of $\gamma = 1.2\hbar\mathring{\omega}_0$. The pairing energy E_p is calculated in the BCS formalism with the strengths:

$$G_p = 19/A \text{ MeV} \quad \text{and} \quad G_n = 14/A \text{ MeV} \tag{8}$$

which are known to fit the empirical odd-even mass differences in the actinides if Z levels for protons and N levels for neutrons are used.[12] The pairing strengths have been made surface dependent.

The use of a potential with infinite depth in Eq. (1) is chosen not only because of convenience but is suggested by the good results for the PES obtained in the Nilsson model.[1] It should also be noted that the use of the Strutinsky prescription is only well defined for the case of potentials without unbound states. In the case of the Nilsson model the appropriate smearing width γ is determined by a stability condition on the shell correction δU. In the case of a finite depth potential, however, such a condition does not exist,[13] and here the shell correction even depends on the size of the basis used for the diagonalization of the single-particle potential if energies in the continuum are taken into account.

III. BARRIERS IN THE $A \simeq 200$ REGION

The two-center model allows the treatment of very constricted shapes, since the basis itself already contains the constriction degree of freedom. Thus it is possible to calculate fission barriers for lighter as well as heavier nuclei in this model. (This has not been possible in the Nilsson model.) The LDM surfaces for the two nuclei ^{202}Pb and ^{212}Rn together with those of the heavier nuclei are shown in Figs. 1 and 2 in a contour line representation. The surfaces are given in a two-dimensional plane consisting of a constriction and an elongation degree of freedom. These are defined with the quantities of Eq. (7) in the following way:

$$l = \frac{z_0 + c}{R}$$

and

$$d = 1 - \frac{d_0}{a} = 1 - \left(1 - \frac{z_0^2}{2c^2}\right)^{1/2}, \tag{9}$$

where d_0 is the absolute neck thickness (see Fig. 4 of Ref. 7). Thus, l gives directly the length of the nuclear shape in units of the radius of the fissioning nucleus. The constriction parameter d is defined in such a way that for $d = 0$ the shapes are pure spheroids, whereas $d = 1$ corresponds to the scission configuration. For values in between, $1 - d$ gives the ratio of the neck thickness to the greatest dimension in the ρ direction.

In Figs. 3 and 4 the corresponding shell-correction energies together with the total PES's are shown for the same two cases. Two of the points in these surfaces are directly comparable with the experimental data: the total shell energy $\delta U + E_p$ at the ground state ($d = 0$, $l = 1$) and the absolute height of the fission barrier above the ground state. The relevant numbers are given in Table II. It is seen, that the theoretical quantities reproduce the experimental numbers[14-16] quite well. Since the barrier heights given here are obtained as the differences between the barrier energies and ground-state energies, it is clear that their inaccuracy is of the same order as that of the ground-state shell energy (which includes both the shell correction δU and the pairing energy). The discrepancy in the ground-state shell energy of 0.3 MeV in the case of ^{202}Pb can presumably not be improved without a simultaneous refit of the total energy formula (6). It turns out that in this case, the pairing energy contributes only 0.3 MeV because of the proton shell closure. Thus the total shell energy is predominantly due to the shell correction δU. In the case of ^{212}Rn the shell correction alone gives exactly the experimental value $\delta U = -7.6$ MeV.[14] Thus the discrepancy between experiment and theory for the ground-state mass is due exclusively to the overestimate in pairing energy, whose strength should perhaps be lowered in future calculations.

For the nucleus ^{202}Pb, however, where the pairing energy is negligible because of the shell closure, the agreement with experiment both for the saddle point and for the ground-state shell energy is very good. We will, therefore, discuss this case in detail in the following paragraphs.

It is seen from Table II that the LDM does not predict the correct barrier heights, mainly because of the large negative shell correction at the ground state originating from the double shell closure at ^{208}Pb. Because of this property Myers and

Swiatecki have fitted their mass formula by using a shell correction which only contributes at the ground state.[11] For this fit the experimental ground-state masses together with the experimental fission barrier of ^{201}Tl,[15] immediately neighboring ^{202}Pb, have been used for the determination of the LDM parameters. Therefore, an investigation of the different contributions to the saddle-point energy and of its properties is interesting.

From Figs. 3 and 4 it can bee seen that the shell-correction energy δU is determined by two dominant features, a large negative value at the spherical configuration ($l=1$, $d=0$) and a distinct valley of approximately -6 MeV going out to scission nearly vertically to the l axis at $l=2.0-2.2$. We will discuss the origin of this structure separately in Sec. V. By comparing the structure in the shell-correction energy δU with the classical fission path over the LDM barrier one can see that this valley in δU leads to a depression of the total potential energy at deformations in the neighborhood of $l=2$. Although this effect is counteracted by the pairing force,[7] the contribution of the pairing term is not large enough to change the depression of the total energy. Since the LDM saddle point lies at $l=1.8-1.9$, the depression of the PES leads to a shift

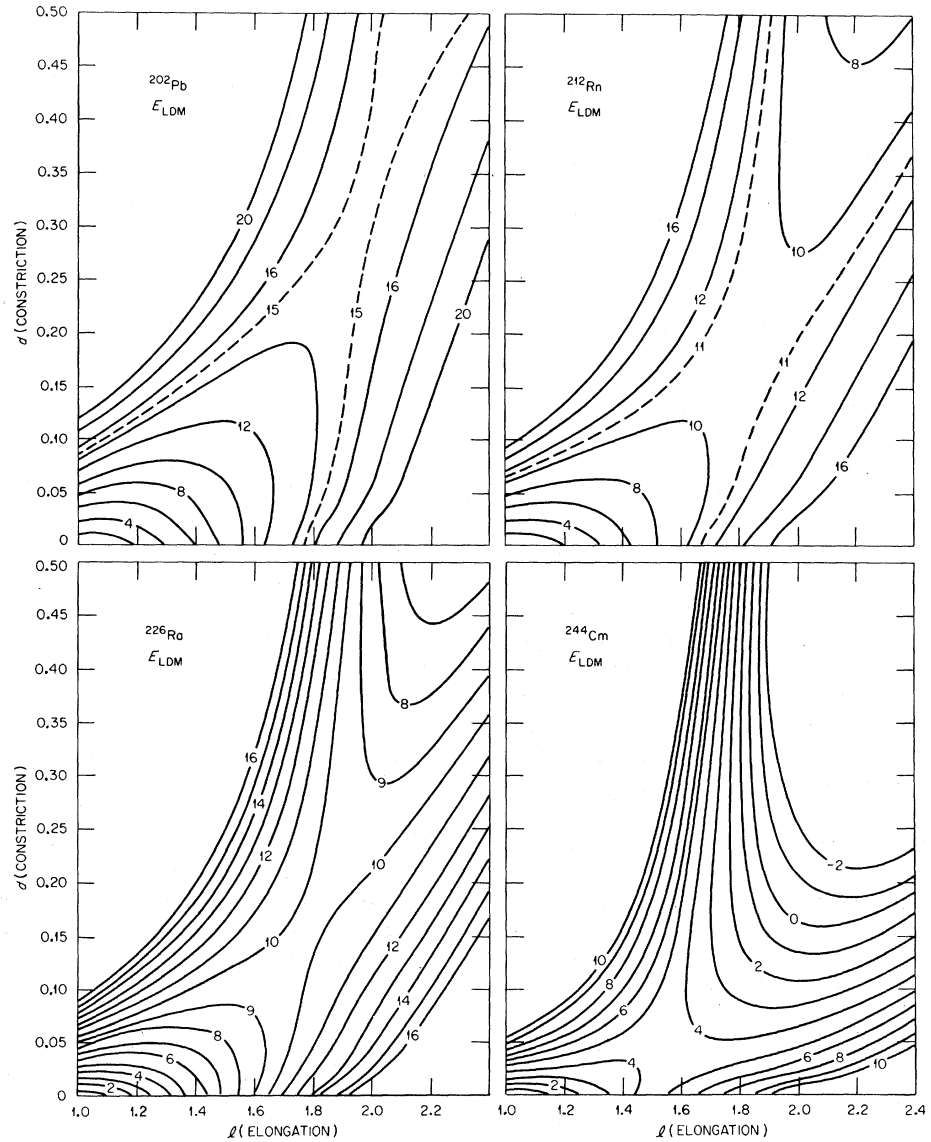

FIG. 1. Liquid-drop-model potential-energy surfaces for the nuclei indicated. The surfaces are given in a two-dimensional representation as a function of the elongation parameter l and the constriction parameter d as defined in Eq. (9). The full contour lines are drawn for energy intervals of 2 MeV in the cases of ^{202}Pb and ^{212}Rn and 1 MeV in all other cases. The numbers at the lines give the energies in MeV.

of the saddle point towards smaller deformations. Figures 3 and 4, compared with the corresponding parts of Figs. 1 and 2, illustrate this effect and Table II lists the coordinates of the saddle point both in the LDM and in the shell-correction model. It is seen that the barrier shapes are appreciably less deformed than in the LDM prediction, particularly in the constriction direction. We have previously made a similar observation for nuclei in the actinide region,[7] although the effect is not as striking there as it is in the lighter-element region because the LDM barriers are already less deformed for heavier nuclei.

This effect, substantiated by the very good agreement for the ground-state corrections and the fission barrier, leads to two consequences: First, it shows that the shell correction at the saddle point is not negligible as has been assumed by Myers and Swiatecki in their mass-formula fit. Table I shows that the single-particle influence at the LDM barrier in ^{202}Pb is −3 MeV. This means that in the Myers-Swiatecki mass formula the LDM contribution to the saddle-point mass of ^{201}Tl might have been underestimated. This incorrect decomposition of the saddle-point mass might thus be responsible for the Coulomb radius discrepancy dis-

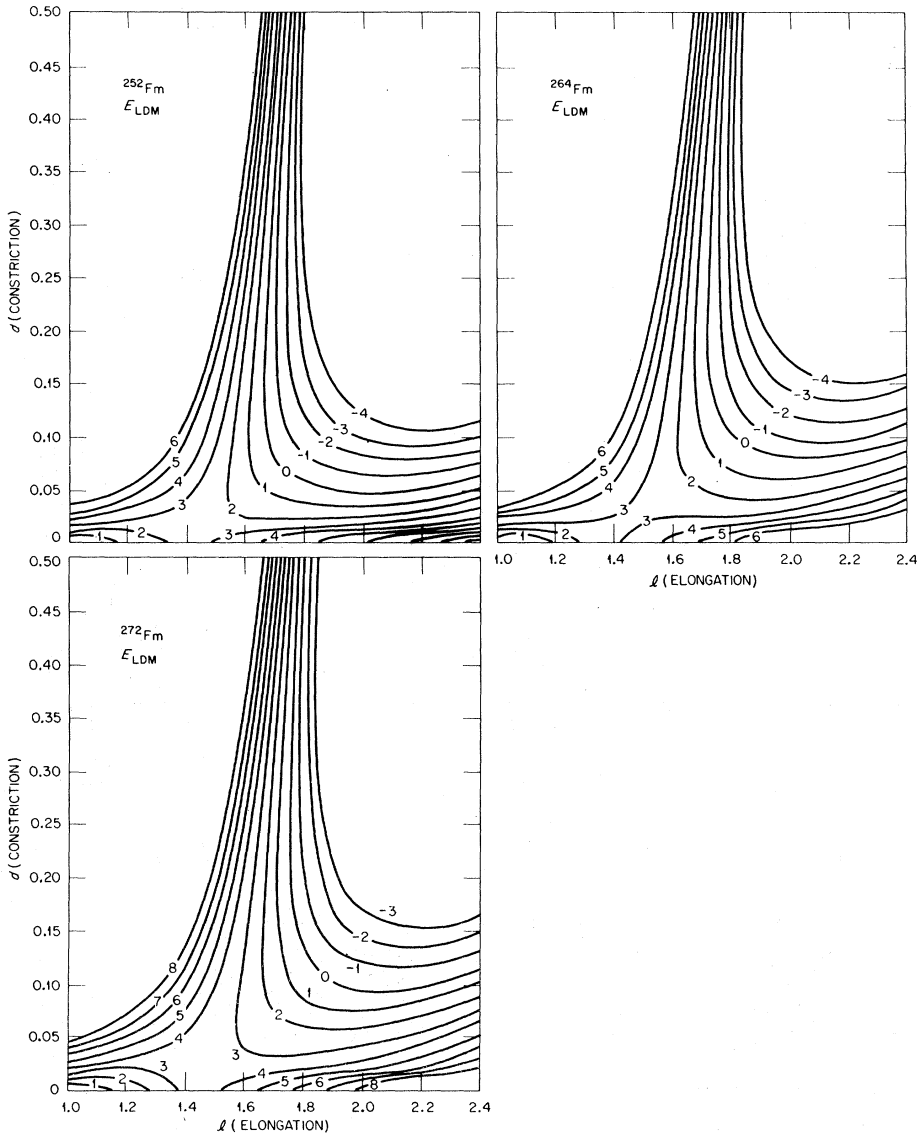

FIG. 2. Liquid-drop-model potential-energy surfaces for the nuclei indicated. The surfaces are given in a two-dimensional representation as a function of the elongation parameter l and the constriction parameter d as defined in Eq. (9). The full contour lines are drawn for energy intervals of 1 MeV. The numbers at the lines give the energies in MeV.

cussed in Ref. 11, since the barrier height was used to fit this parameter in the mass formula.

The second consequence is that the success of the LDM in describing the fission-fragment properties (mass and energy distributions) for lighter nuclei now becomes somewhat accidental. The LDM calculations are rather insensitive to the position of the total barrier and depend almost entirely on the normal modes not leading to fission at the saddle point, which is taken to be the starting point in the dynamic LDM calculations.[17] Since the fragment-shell effects for lighter fissioning nuclei are smaller in absolute magnitude than for heavier nuclei and are relatively smooth, the normal modes orthogonal to the fission coordinate may not be very different in liquid-drop and shell-correction model calculations.

Finally, in the PES's of both ^{202}Pb and ^{212}Rn, second minima appear at an excitation energy of about 12 MeV at an elongation of $l \cong 1.3$–1.4. These minima have already been observed by Tsang[18] in calculations which, however, could not be carried out to the saddle point. Our calculations show that these indeed are stable minima in the PES's, whose origin is the same as that of the second minima in the PES's of heavier nuclei. Since, however, the barriers behind these minima are rather high, effects of these minima will not be observable in fission. Because of their small separations from the ground-state minima, by a barrier height of only 2 MeV, it is also questionable whether the minimum is deep enough or broad enough to support any observable quasibound state. Only dynamic calculations[19] will be able to answer this question.

IV. FISSION BARRIERS IN THE HEAVY-ELEMENT REGION

Figures 5–11 give fission barriers for nuclei in the heavy-element region. Some differences compared with our earlier calculations[7] can be seen. The second minimum is now slightly necked in and the second barrier also appears at larger constrictions. These constrictions, however, are still very small, the constriction parameter d for the second saddle being only $d \simeq 0.1$ for all nuclei from Ra to Cm. Thus here again the shell corrections to the LDM PES lead to a shifting of the saddle point towards smaller deformations. For ^{226}Ra, for example, the LDM saddle lies at $d = 0.175$,

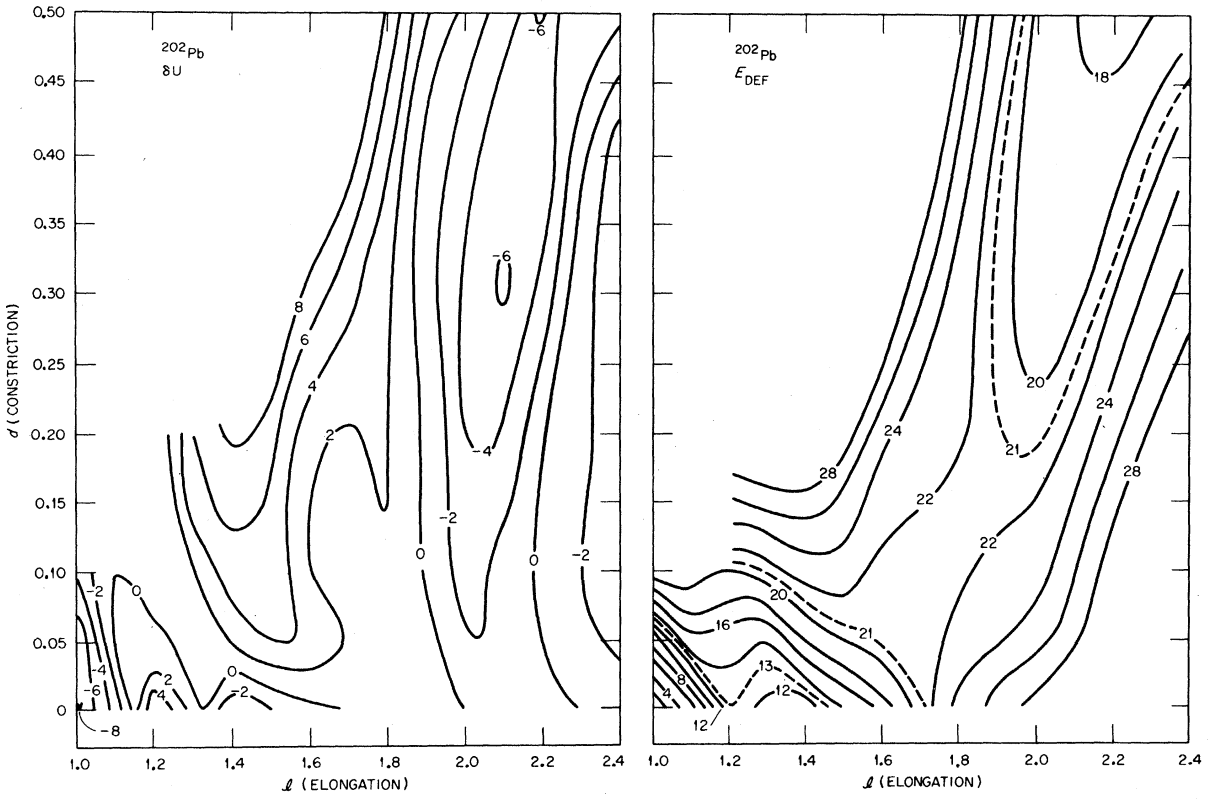

FIG. 3. Shell-correction energy (δU) and potential-energy surfaces (E_{DEF}) for ^{202}Pb. Full contour lines are drawn for energy intervals of 2 MeV. The numbers at the lines give the energies in MeV. The E_{DEF} surface is normalized to zero at $d = 0$, $l = 1$.

$l = 1.8$, whereas the shell-corrected saddle appears at $d = 0.1$, $l = 1.7$. This effect becomes smaller when going to the heavier nuclei, since in these nuclei the LDM saddles already appear at small deformations. The energies of the two saddle points and the second minima are now in rather good agreement with the Nilsson-model predictions[1] although in that work no fragment influences were specifically taken into account and calculations farther along toward scission could not be made. The transition from cases with a higher first barrier towards those with a higher second barrier, which occurs between Cm and Cf as indicated by experimental angular-distribution measurements,[20] is reproduced well. The absolute heights of the second barrier, compared with the experimental values, are too high, very likely because of the neglect of asymmetric configurations, as indicated by recent calculations in which asymmetric degrees of freedom were included.[3]

It is seen in the figures that generally the minimum-potential-energy path to scission consists of an initial elongation, with only little constriction up to the second saddle, then bends over to the direction of increasing constriction, with little further elongation. (Exceptions are ^{244}Cm, ^{248}Cf, and ^{252}Fm.) The shapes corresponding to the stationary points in the PES are shown in Fig. 12 in order to give a feeling for the deformations under discussion.

The shell corrections δU are shown in Figs. 7–11 for ^{226}Ra, for ^{244}Cm, and for three Fm isotopes. The ^{226}Ra shell corrections (Fig. 7) have a ridge at $l \cong 1.6$, which can also be seen in ^{202}Pb (Fig. 3) and ^{212}Rn (Fig. 4). In addition, an indication of a valley appears at $l \cong 1.3$ which leads to a bending over of the PES contour lines just above the position of the second minimum. This PES feature can also be seen in ^{232}Th, ^{236}U, and ^{242}Pu.

For the ^{244}Cm case (Fig. 8) the shell correction δU has now developed a distinct valley at $l = 1.3$–1.5, whereas the ridge around $l \cong 1.6$ has almost disappeared. A second valley appears at $l \cong 1.9$, $d \cong 0.4$. The presence of the first valley causes a significant broadening of the second saddle in the PES, towards larger constrictions.

In ^{252}Fm (Fig. 9) the picture has qualitatively changed. The valley in δU at $l = 1.4$–1.5 now has a

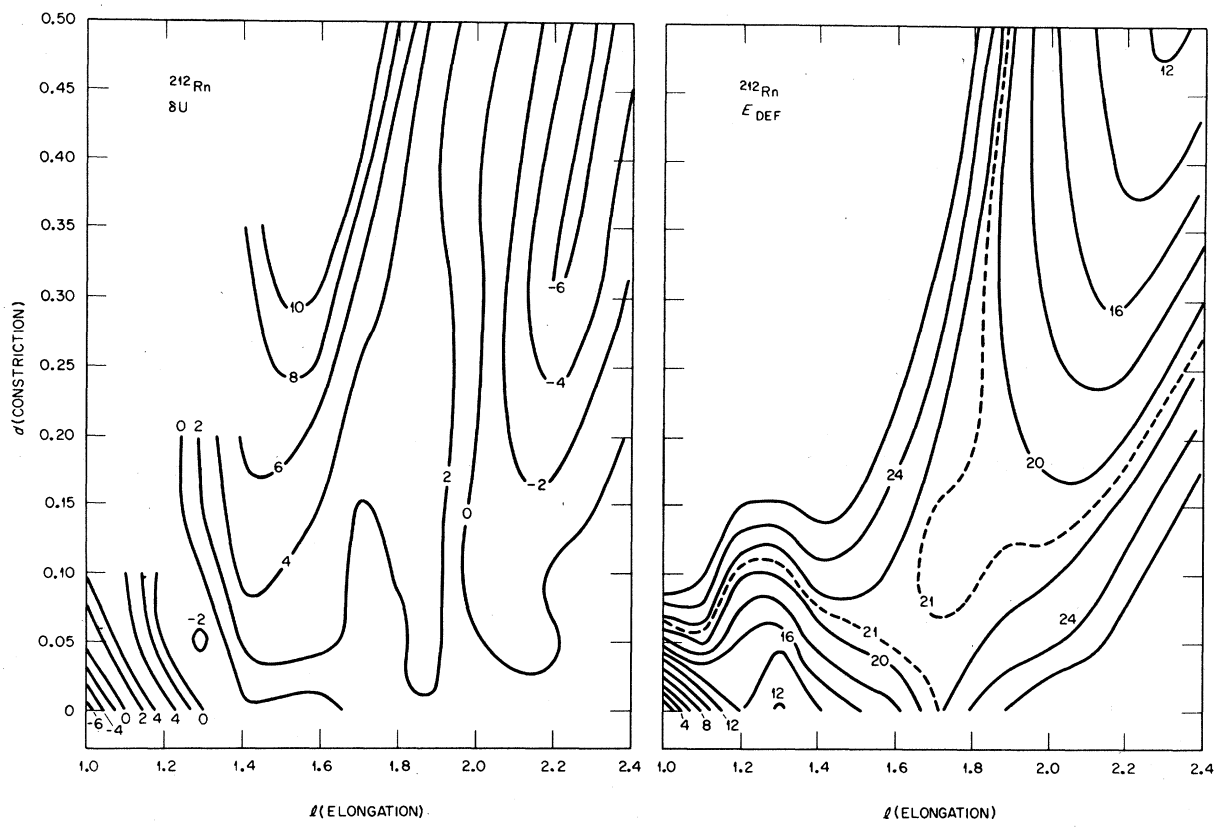

FIG. 4. Shell-correction energy (δU) and potential-energy surfaces (E_{DEF}) for ^{212}Rn. Full contour lines are drawn for energy intervals of 2 MeV. The numbers at the lines give the energies in MeV. The E_{DEF} surface is normalized to zero at $d = 0$, $l = 1$.

TABLE II. The table lists the essential quantities for two nuclei in the $A=200$ region. $E_{s,\,\mathrm{exp}}$ (g.s.) is the experimental shell-correction energy at the ground state as determined in Ref. 14, δU gives the theoretical shell correction (without pairing) at the ground state, E_p (g.s.) the pairing correction energy there, and E_s (g.s.) finally the total single-particle correction at the spherical ground state. E_B (exp) lists experimental fission barriers determined for the neighboring nuclei indicated, E_B (LDM) gives the LDM prediction for these barrier heights in the shape parametrization used in this paper, and E_B the total theoretical shell-corrected fission barrier. E_s (saddle) represents the total shell correction ($\delta U + E_p$) at the LDM saddle, P_{LDM} gives the position (l, d) for the fission barrier in the LDM, and P the position of the same barrier as obtained in the shell-corrected calculations. All energies are given in MeV.

	$E_{s,\mathrm{exp}}$ (g.s.) [a]	δU (g.s.)	δE_p (g.s.)	E_s (g.s.)	E_B (exp)	E_B (LDM)	E_B	E_s (saddle)	P_{LDM} (l, d)	P (l, d)
^{202}Pb	−7.9	−7.9	−0.3	−8.2	22.5 ± 1.5 [b]	14.9	21.5	−3.0	(1.9, 0.3)	(1.8, 0.15)
^{212}Rn	−7.6	−7.3	−2.2	−9.5	18.6 ± 2 [c]	10.2	21.2	−0.5	(1.8, 0.2)	(1.7, 0.05)

[a] Myers and Swiatecki, Ref. 14.
[b] Burnett *et al.*, Ref. 15. Barrier of ^{201}Tl.
[c] Huizenga, Chaudry, and Vandenbosch, Ref. 16. Barrier of ^{210}Po.

depth of −12 MeV at $d=0.5$ and is strong enough at smaller constrictions to determine the structure and the position of the second minimum and the second saddle in the PES. The second minimum is now extended along the constriction axis, and the fission path already bends over toward constriction at the first barrier, so that on the way from the second minimum to the second barrier the elongation of the nuclear shape changes very little. The same behavior also appears in the heavier nuclei ^{264}Fm (Fig. 10) and ^{272}Fm (Fig. 11).

In ^{264}Fm the valley in δU has a depth of −22 MeV at $d=0.5$ and is strong enough to alter the PES significantly, compared with the other cases. We have here (Fig. 10, E_{DEF}) two well-separated paths from the first saddle to scission. One is given by the usual LDM behavior and is characterized by a gradual increase both of l and d (compare Fig. 2, E_{DEF} for ^{264}Fm). The other, caused by the structure in δU, goes vertically upward from the saddle

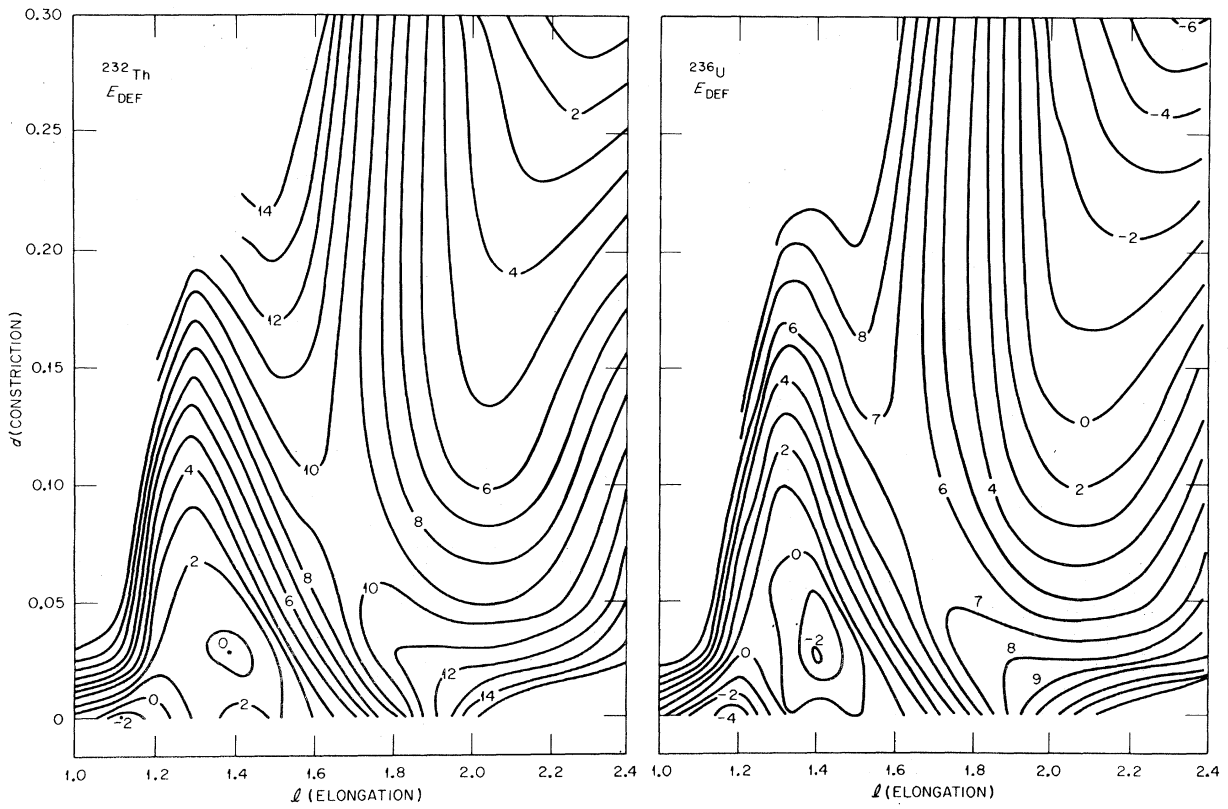

FIG. 5. The potential-energy surfaces for ^{232}Th and ^{236}U. The contour lines are drawn at intervals of 1 MeV. The surfaces are again normalized to zero at the spherical shape ($d=0$, $l=1$).

with almost no increase in elongation at all. Only at $d \simeq 0.5-0.6$ does this valley join the LDM valley. In ^{272}Fm (Fig. 11) the same effect can be seen though a little less pronounced.

Thus we have observed gradual but distinct changes in the structure of the PES with increasing Z and A of the compound nucleus, from ^{226}Ra through the Fm isotopes to ^{272}Fm.

In order to show that the structure of the PES's is independent of the specific pairing treatment and depends only on the shell correction δU, we have carried out a calculation with a constant, surface-independent pairing strength G for ^{264}Fm. The result is shown in Fig. 13. It is seen that indeed the general features of this PES compared with that of Fig. 10 do not change.

V. FRAGMENT-SHELL INFLUENCES

In Secs. III and IV we have seen that the character of the PES changes gradually when going from the Pb region to the very heavy Fm isotopes. This change is ascribed principally to corresponding changes in the shell corrections δU. The surfaces of the quantity δU are characterized by pronounced structure in certain regions and rather diffuse behavior in others.

In order to summarize the distinct features here once more for easier reference (see Figs. 3, 4, and 7–11), we see that in the Pb region the δU surfaces show a ridge around the elongation $l \cong 1.4-1.5$ and a valley at $l = 2.1-2.2$, the energy of which is approximately -6 MeV at $d = 0.5$. In ^{226}Ra the valley at $l = 2.2$ has disappeared, whereas the ridge at $l = 1.6$ still appears. Also an indication of a valley begins to develop at $l = 1.2-1.3$. This valley, now shifted to $l \cong 1.4-1.5$ has become the dominant structure in ^{244}Cm, with an energy of -7 MeV at $d = 0.5$. In addition a second, shallower valley at $l \cong 1.8-1.9$ appears. The ridge at $l \cong 1.6$ has become much less pronounced. When going through the Fm isotopes, the valley at 1.4–1.5 becomes deeper from ^{252}Fm to ^{264}Fm and then shallower again in ^{272}Fm. The values at $d = 0.5$ are -13 MeV for ^{252}Fm, -22 MeV for ^{264}Fm, and -15 MeV for ^{272}Fm. At the same time it is seen that a ridge at $l \cong 2.0$ is built up in all of the Fm isotopes. In all cases, the dominant structures, i.e., the ridges and valleys, begin at small d values, $d \lesssim 0.1$ (see Figs. 3, 4, and 7–11).

In order to understand the origin of this structure in δU (and thus also in the PES) and its gradual change with Z and A of the compound nucleus,

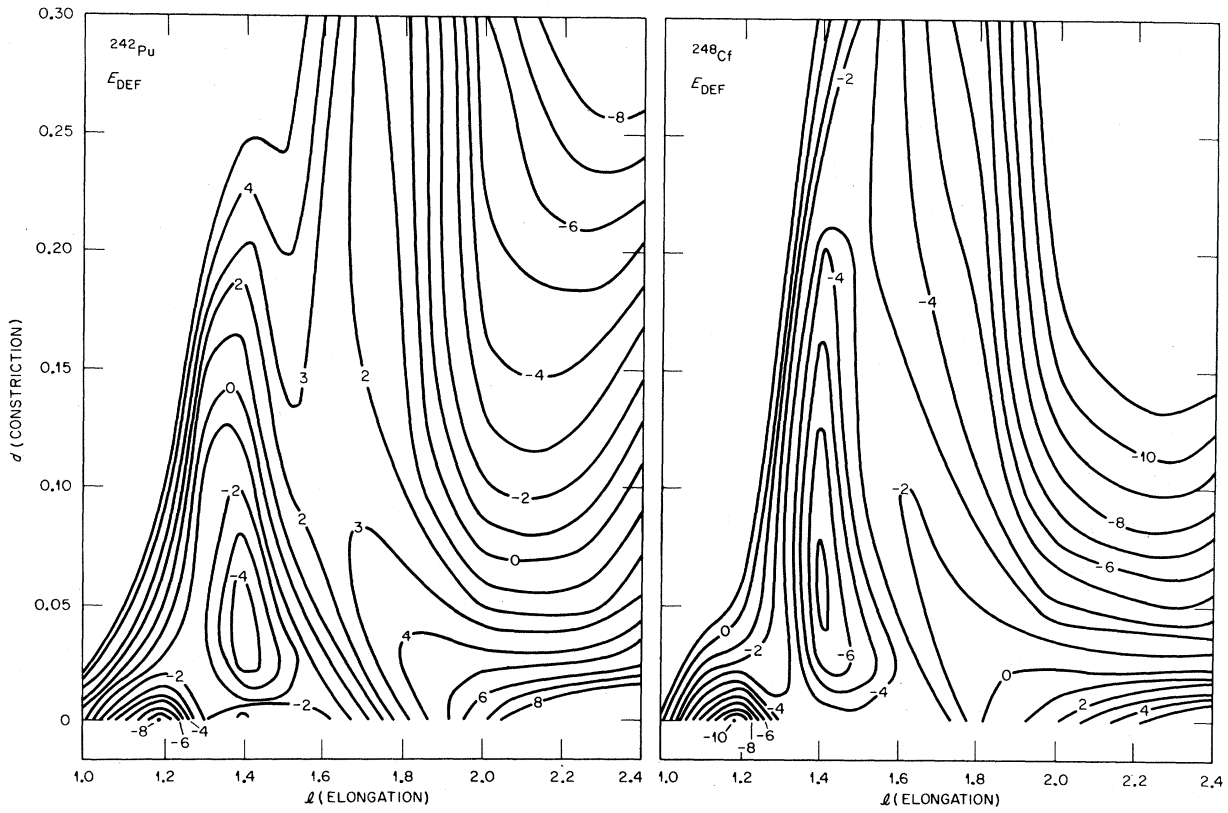

FIG. 6. The potential-energy surfaces for ^{242}Pu and ^{248}Cf. The contour lines are drawn at intervals of 1 MeV. The surfaces are again normalized to zero at the spherical shape ($d = 0$, $l = 1$).

we have analyzed the single-particle states in these regions with respect to their degeneracy. Since at the scission point, or immediately afterward, two identical shell-model potentials must be present, the single-particle energies will be degenerate in pairs of states with different parity. A direct linear combination of these two wave functions then yields states that are localized in one or the other of the two fragments.[7] Thus the degree of degeneracy of two states is a direct indication of the degree of preformation of the fragment shells. Such an analysis for ^{236}U[7] and ^{202}Pb shows that at $d \cong 0.4$ the violation of degeneracy of states at the Fermi surface is already less than 1 MeV, thus indicating a considerable degree of preformation. This finding strongly suggests that the structure of the δU surfaces is due to fragment-shell influences.

A direct test of fragment-shell influence may be made by comparing the structure in the δU surfaces at large d values (e.g., $d \cong 0.5$) with shell corrections calculated for independent-fragment nuclei. For this purpose, it is desirable to use a shape parametrization for the individual fragments in which perturbations of the single-particle levels due specifically to nuclear interactions at the neck are removed, but with the over-all shape distortions (due to the mutual Coulomb interaction) maintained. A reasonable approximation which meets these requirements consists of two tangent spheroids.

The connection between the deformation p of the single fragments (p = ratio of major to minor axis of the spheroid) and the elongation l of the compound-nucleus shape is

$$l = (2p)^{2/3} . \tag{10}$$

The configuration of two touching spheres in this model is thus at $l_0 = 2^{2/3} \approx 1.58$, that of two touching oblate spheroids is at $l < l_0$, and that of two touching prolate spheroids is at $l > l_0$. We refer to this model as the independent-fragment model (IFM).

In Fig. 14 we show, as a function of l, the total shell correction δU obtained in the IFM calculations, in comparison with the shell correction δU calculated for $d = 0.5$ in our realistic model with the Hamiltonian of Eq. (1). The solid curves show δU for the realistic model and are obtained direct-

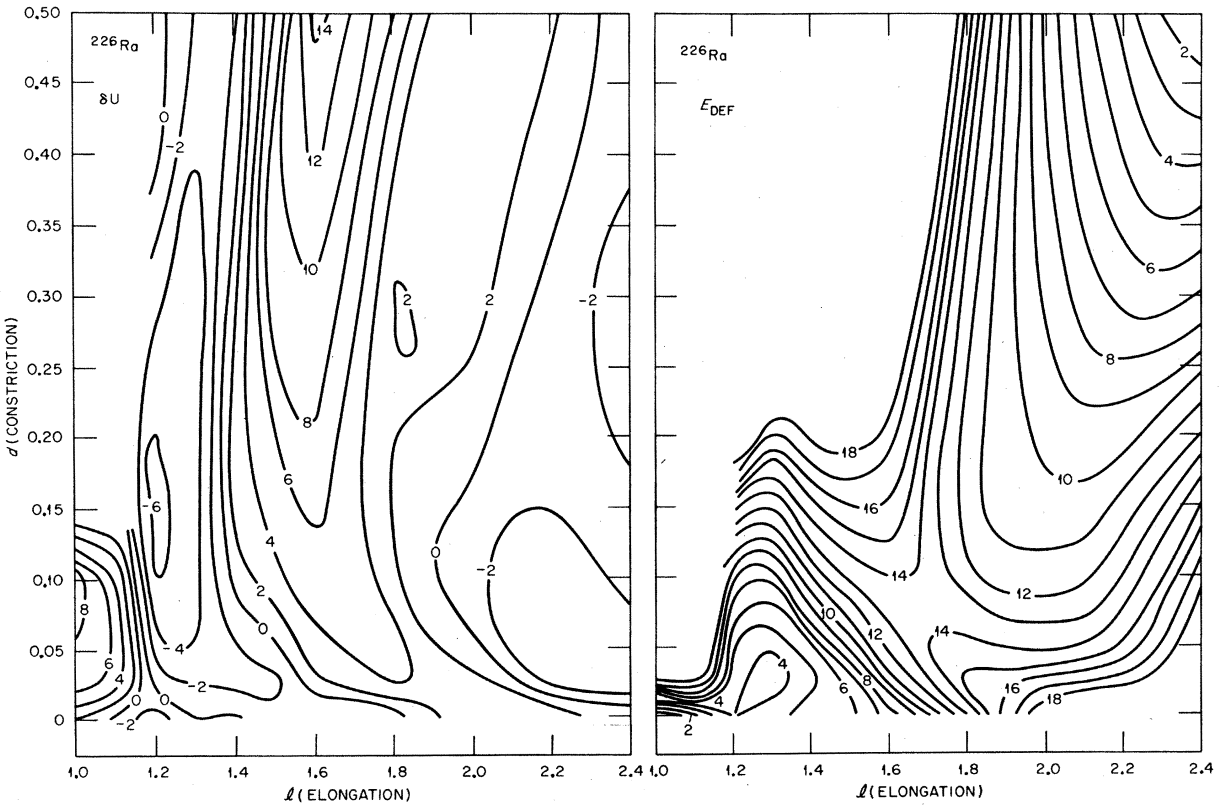

FIG. 7. Shell-correction energy (δU) and potential-energy surface (E_{DEF}) for ^{226}Ra. The contour lines for δU are drawn at intervals of 2 MeV, for E_{DEF} at intervals of 1 MeV. The numbers at the curves give the energies in MeV. The PES is normalized to zero for the spherical shape ($d = 0$, $l = 1$).

ly from Figs. 3, 4, and 7–11. They correspond to cuts in these figures yielding δU vs l at $d=0.5$. The dashed curves show δU vs. l for the IFM.

The agreement found is surprisingly good in all cases. We shall discuss the results and their interpretation for each case separately:

^{202}Pb. The dominant structure in the realistic δU are a high maximum at $l\cong 1.6-1.7$, corresponding to the ridge in the δU surface, and a minimum at $l\cong 2.2$. Both structures are also present in the IFM calculation and reflect the fact that nuclei in the region around $A\cong 100$ are permanently deformed midshell nuclei.[10,21] They have, therefore, large positive shell corrections at the spherical shape and negative δU values for deformed shapes. The minimum at $l\cong 2.2$ has a depth of -6 MeV and a maximum at $l=1.6-1.7$ has a height of 21 MeV in the realistic shell correction.

^{212}Rn. The maximum at $l\cong 1.6-1.7$ in the realistic shell correction has decreased to 16 MeV, and the flat minimum at $l\cong 2.3$ where $\delta U=-6$ MeV is still present. Also the decrease of the maximum towards large elongations is quite slow. The IFM predicts a maximum of 17 MeV at $l\cong 1.6$, a first shallow minimum of -2 MeV at $l\cong 1.9-2.0$, a second very small maximum of 3.5 MeV at $l\cong 2.1-2.2$, and a second minimum at $l\gtrsim 2.4$. This rather smooth structure of δU at $l\gtrsim 1.9$ corresponds to the slow decline of the maximum in the realistic δU toward larger elongations. The IFM also yields a very shallow valley at $l\simeq 1.3$ corresponding to two oblate spheroids.

^{226}Ra. The shallow valley corresponding to oblate spheroids in the IFM is now shifted slightly to higher elongations ($l\cong 1.3-1.4$) and has become somewhat deeper (-1.5 MeV). It corresponds to the weak indication of a valley at $l\cong 1.3-1.4$ in the realistic δU surface (see Fig. 7) which has a minimum of -3 MeV at this location. The maximum at $l\cong 1.6$ is still present, although it is weaker in the realistic calculation than in the IFM. The IFM also shows a minimum of -1.5 MeV at $l\cong 1.9$ which, however, corresponds only to a flattening of δU in the realistic calculation. The transition from Rn to Ra is thus marked by the disappearance of the valley in δU at $l\cong 2.2$ and the appearance of a new valley at $l\cong 1.3-1.4$. This change reflects the energetic preference of the oblate (rather than pro-

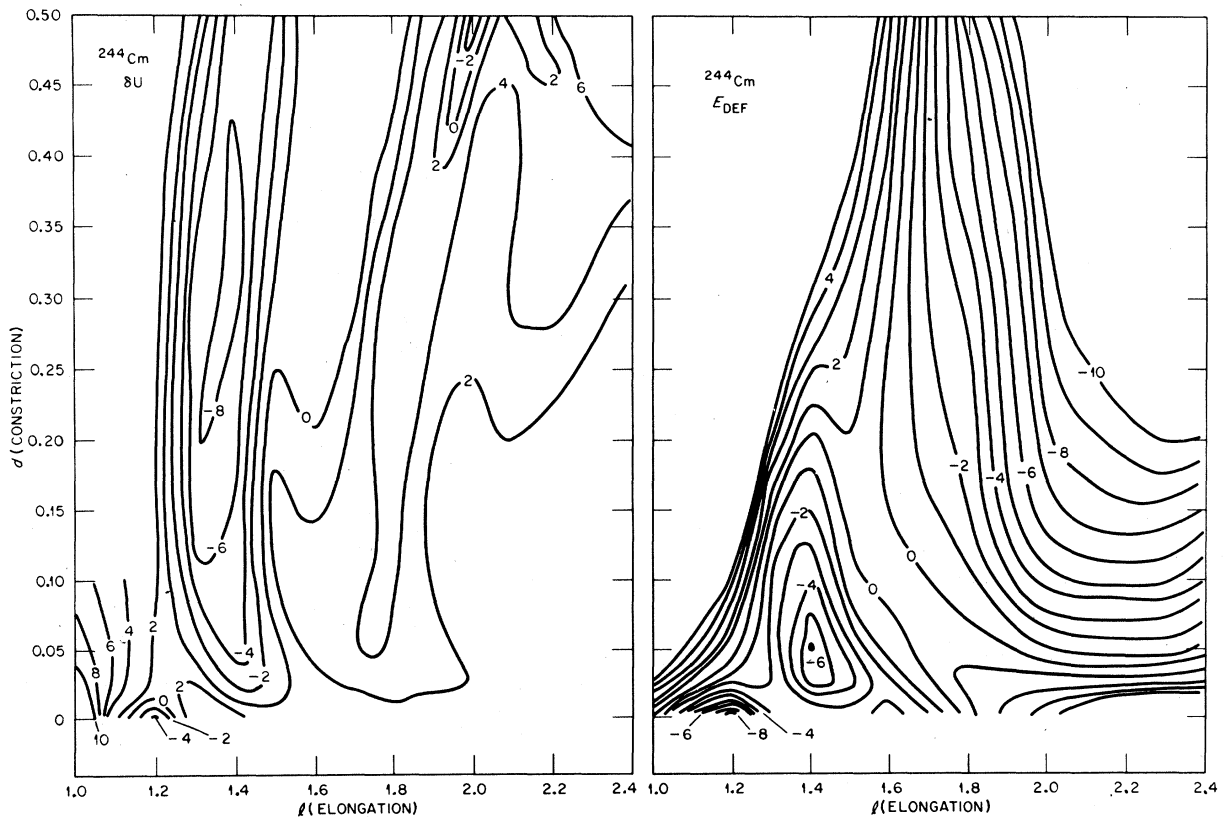

FIG. 8. Shell-correction energy (δU) and potential-energy surface (E_{DEF}) for ^{244}Cm. The contour lines for δU are drawn at intervals of 2 MeV, for E_{DEF} at intervals of 1 MeV. The numbers at the curves give the energies in MeV. The PES is normalized to zero for the spherical shape ($d=0$, $l=1$).

late) minimum in the IFM calculation for certain nuclei in the $A \approx 100$ region. (Earlier theoretical calculations indicate that nuclei in this region may have stable oblate deformations[10] in their ground states.)

^{244}Cm. The minimum occurring at $l \cong 1.4-1.5$ in the realistic shell correction has shifted to slightly larger elongations relative to ^{226}Ra, and has a depth of −8.5 MeV. The maximum of 0.6 MeV at $l = 1.6$ is weaker here than in ^{226}Ra. The minimum in the realistic δU at $l \cong 1.8$ is rather weak (−2.5 MeV), relative to the IFM prediction (−8 MeV). The over-all structure, however, as indicated by the positions of the two minima and the maximum, is again well reproduced.

Fm. In these isotopes we have fragment nuclei with the magic proton number $Z = 50$, for which the proton shell correction is large and negative at $p = 1$ ($l \cong 1.58$). For this reason the maximum at $l \cong 1.6$ has now disappeared in the realistic δU for ^{252}Fm and is seen only very weakly in the IFM calculation. The largest value of the shell correction of −30 MeV is reached for ^{264}Fm, which can fission symmetrically into two doubly magic $^{132}_{50}Sn_{82}$ nuclei. Both ^{252}Fm and ^{272}Fm, below and above this special configuration, respectively, have shallower minima at $l \cong 1.6$ because of the nonmagic fragment neutron numbers. The absolute minimum for ^{252}Fm occurs at $l = 1.5$ with $\delta U = -13$ MeV, shifts to $l \cong 1.6$ with $\delta U = -23$ MeV for ^{264}Fm, then shifts somewhat further to $l \cong 1.65$ with $\delta U = -17$ MeV for ^{272}Fm. The predictions of the IFM for the Fm isotopes are directly understandable in terms of the double shell closure at $A = 132$ and are in excellent agreement with the realistic calculations.

These comparisons show conclusively that the magnitudes and mass dependences of the structures in the shell corrections δU are specifically linked to the fragment shells, and show further that the specific structure in the shell-correction surfaces as described in the first two paragraphs of this section are indeed due entirely to fragment-shell effects. The gradual change from Pb to Fm, i.e., the disappearance of the ridge at $l \cong 1.6$ and the valley at $l \cong 2.2$ and the development of a new valley at $l = 1.2$ which then shifts with increasing mass to $l = 1.4-1.6$, thus reflects the transition from a fragment formed in a midshell region, through fragments formed in a region where the ground-state nuclei may have oblate shapes, to

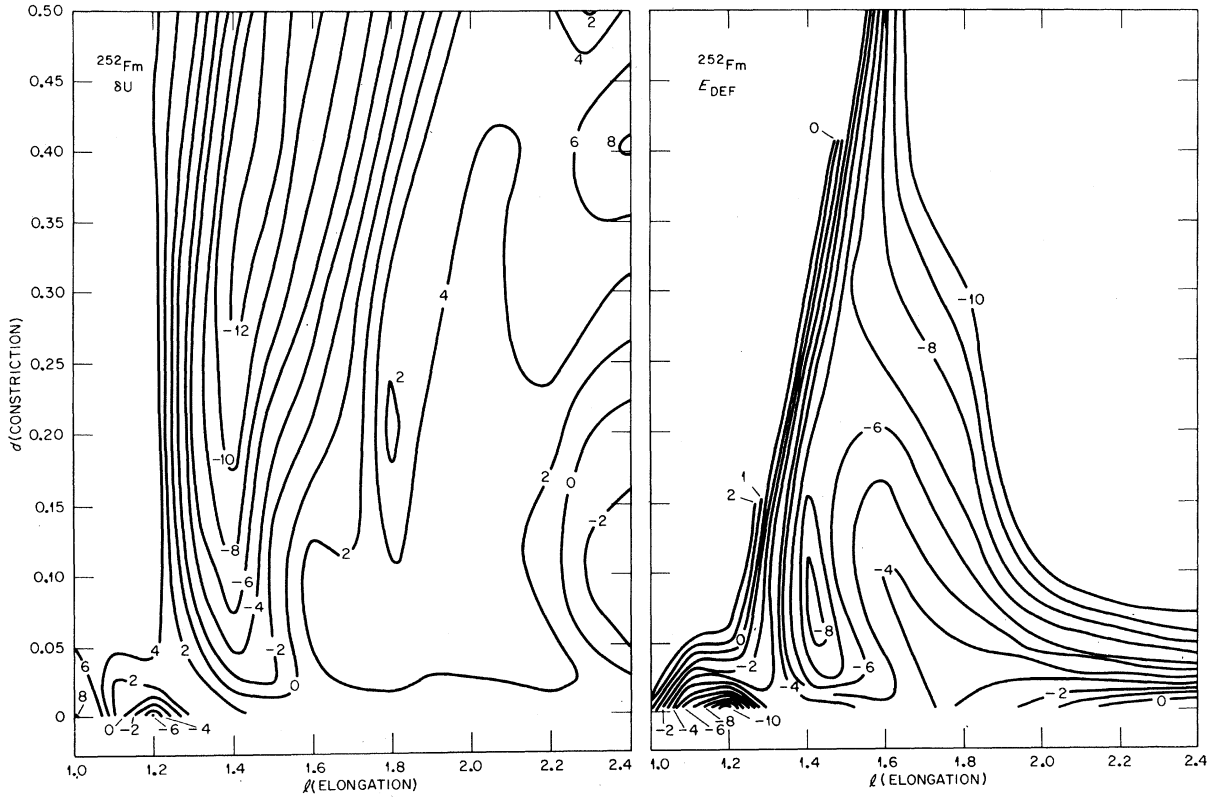

FIG. 9. Shell-correction energy (δU) and potential-energy surface (E_{DEF}) for ^{252}Fm. The contour lines for δU are drawn at intervals of 2 MeV, for E_{DEF} at intervals of 1 MeV. The numbers at the curves give the energies in MeV. The PES is normalized to zero for the spherical shape ($d = 0$, $l = 1$).

fragments formed in a doubly magic region. We stress again that this structure in the shell corrections appears very early, at constrictions as small as $d \cong 0.1$, where very little necking in is present in the nuclear shape (see Fig. 12).

It is of interest that the elongations l, at which the structures showing fragment-shell influence appear, correspond approximately to the positions of the second minima in the PES's. These minima, however, occur for constrictions near $d = 0$ and are mainly determined by the compound-nuclear structure, in particular by the second minimum in the usual compound-nucleus shell correction. Thus, the coincidence in l values between the minima in the shell corrections for the compound nucleus and for the two-fragment system seems to be accidental. (Fragment shells may, however, influence the structure of the second minimum somewhat, especially in the heavier nuclei where they lead to a distinct change in the fission path from the second minimum onward.)

VI. CONCLUSIONS AND CONSEQUENCES FOR NUCLEAR FISSION

The present work, including that described in our first report,[7] is an attempt to investigate the potential surface for fissioning nuclei in a realistic model, from the ground state of the compound nucleus almost to the scission point. It is our aim to provide an understanding of the structures observed in these surfaces, with particular attention to their correlation with fragment properties, to determine the extent to which the nascent fragments might be preformed at the saddle point and in the descent from the saddle point to scission.

Although our calculations are limited to symmetric configurations, the qualitative features of the results are expected to apply equally well to asymmetric configurations, since the preformation mechanism is similar in the two cases.[22] In fact, since the shell-correction energies increase for nuclei in the region of doubly magic $^{132}_{50}Sn_{82}$, the effect of asymmetry in heavier compound nuclei ($A \gtrsim 230$) should be to enhance fragment-shell effects on the compound-nucleus PES.

The results of this study give some rather new and basic insights into the mechanism of fission, and provide a framework within which a variety of earlier ideas and experimental observations may be reconciled. The validity (or lack of validity) of

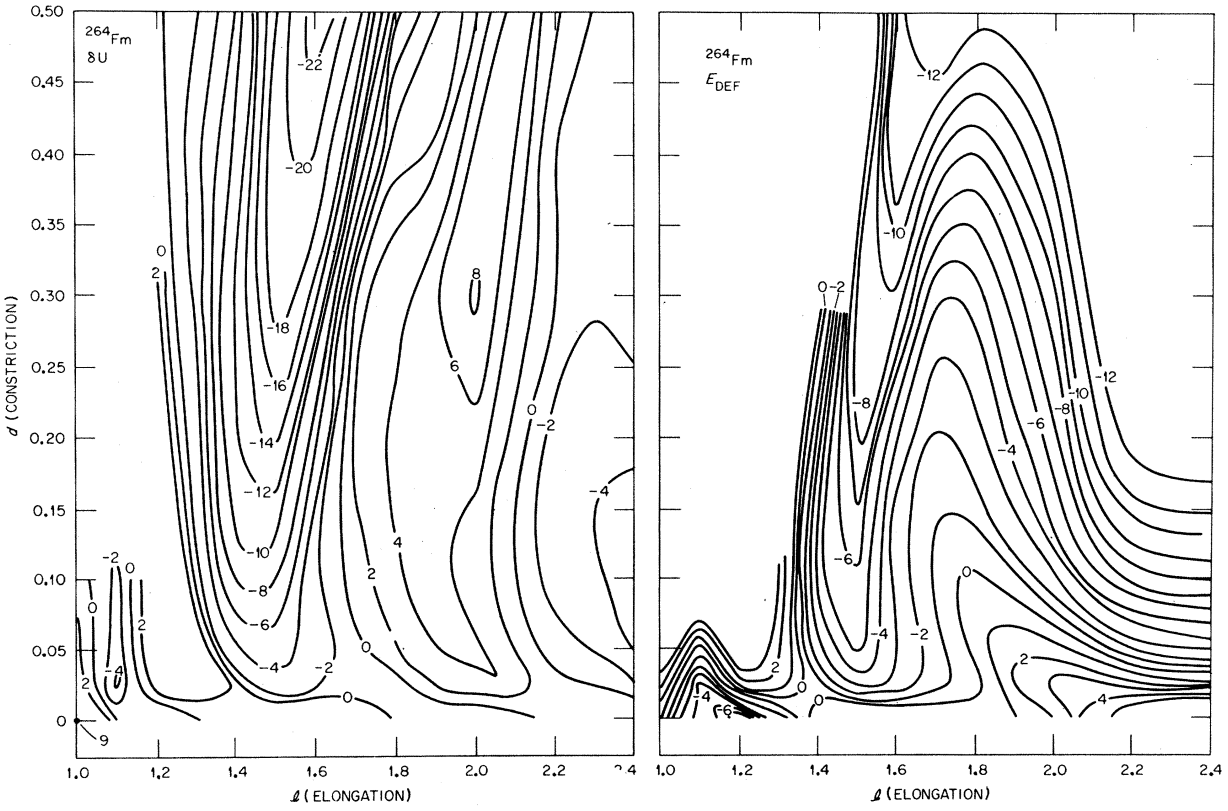

FIG. 10. Shell-correction energy (δU) and potential-energy surface (E_{DEF}) for ^{264}Fm. The contour lines for δU are drawn at intervals of 2 MeV, for E_{DEF} at intervals of 1 MeV. The numbers at the curves give the energies in MeV. The PES is normalized to zero for the spherical shape ($d = 0$, $l = 1$).

previous theoretical approaches to fission now also becomes clear in this framework.

Before beginning our discussion along these lines we should perhaps point out that conclusions based on potential-energy surfaces alone necessarily imply a static approximation for the fission process, since they neglect the influence of the mass parameters associated with collective motion along the fission potentials. It is possible that these mass parameters have an influence on the fission process,[23] e.g., they may influence the path on the PES in such a way that it may not coincide with the minimum-potential-energy path. It is well known, however, that the mass parameters also exhibit shell effects.[24] Since we have seen that the single-particle states approach those of two separated fragments very early, the mass parameters themselves should also approach their values for the fragments rather early along the fission path. Therefore the fragment-shell influences before scission should be even stronger in dynamical calculations. This argument, in effect, strengthens the conclusions we shall draw on the basis of PES's. Furthermore, the conclusions we shall discuss are independent of model details (e.g., specific choice of l-dependent terms in the Hamiltonian, etc.).

Basic results. Our basic finding in this work is that, for the entire range of heavy nuclei $A \gtrsim 200$ and for constrictions $d \gtrsim 0.1$, the structure in the realistic potential-energy surface is essentially determined by the combination of specific nuclear-structure properties of the nascent fragments and the LDM potential surface. That is to say, the specific nuclear-structure properties (e.g., shell energies) of the free individual fragments are reflected in the realistic compound-nucleus PES and are important from the scission line ($d = 1.0$) inward to constrictions as small as $d \cong 0.1$. (See Secs. IV and V.)

In the region of small constriction ($d \lesssim 0.1$) the structure of the realistic PES is determined essentially by the nuclear-structure properties (e.g., shell energies) of the compound nucleus as determined in the usual Nilsson model by Nilsson[1] and Strutinsky[1,2] with LDM normalization.

Barrier heights. The fission-barrier heights obtained in this work for compound nuclei in the re-

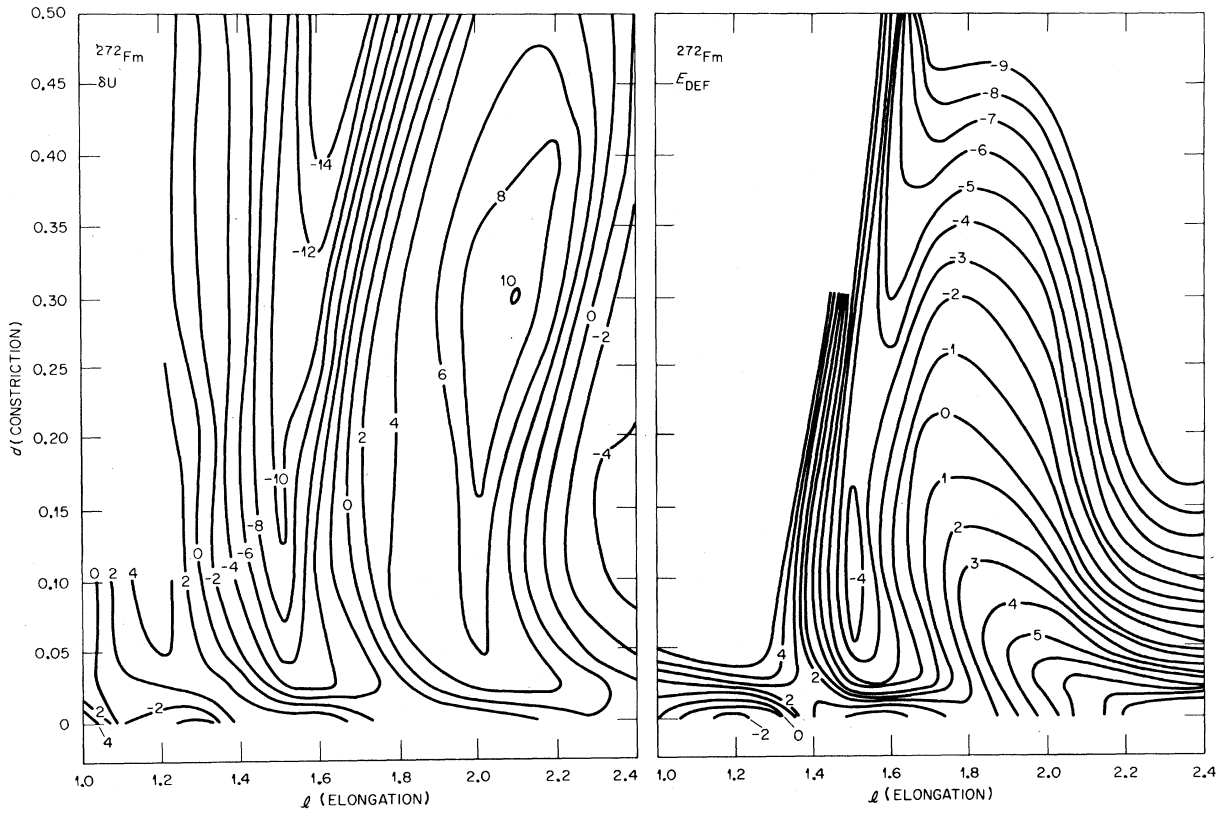

FIG. 11. Shell-correction energy (δU) and potential-energy surface (E_{DEF}) for ^{272}Fm. The contour lines for δU are drawn at intervals of 2 MeV, for E_{DEF} at intervals of 1 MeV. The numbers at the curves give the energies in MeV. The PES is normalized to zero for the spherical shape ($d = 0$, $l = 1$).

gion $A \cong 200$ agree well with experimental values. In addition, the calculated total shell-plus-pairing-energy correction for the ground state agrees with experiment.

The coordinates of the calculated barrier are not the same as those of the LDM barrier. In the realistic calculations we obtain much smaller constrictions (d values) and slightly smaller elongations (l values) than are given by the LDM. That is, the saddle-point shapes are much less constricted (necked in) than has been previously supposed from LDM calculations.

In spite of this, the minimum-potential-energy path to scission is not changed appreciably. Thus for these nuclei ($A \cong 200$) we conclude that the chief effect of the fragment shells on the fission barrier is to change its position and magnitude (relative to the LDM), but in such a way that the fission path remains almost unchanged.

Barrier heights obtained for compound nuclei in the region $A \gtrsim 230$ are somewhat higher than experimental values. This result is understandable, however, both from our basic results as described above and from earlier calculations of Möller and Nilsson[3] which yield lower second-barrier heights for asymmetric shapes than for symmetric shapes, for compound nuclei with $A \gtrsim 230$.

As indicated above, when nascent fragment nuclei are in the region of $Z \cong 50$, $N \cong 82$ in an asymmetric configuration, the effects of fragment shells on the PES are expected to be enhanced relative to the symmetric configuration. It is almost surely the case that the effect observed by Möller and Nilsson is a direct result of fragment-shell effects which are sufficiently strong in this case to affect the height of the second barrier in the PES. It is clear that this leads to a preference for asymmetric fission, but further quantitative calculations are necessary to determine whether the correct maximum yield at fragment mass ~140 amu (not 132 amu) is predicted for the lighter actinides ($230 \lesssim A \lesssim 252$).

Fragment Mass and Energy Distributions

1. $A \cong 200$. It was found by Nix and Swiatecki[17] that the fission properties of nuclei in this mass region could be reasonably well reproduced by the LDM, completely without shell effects, even though the calculated LDM saddle-point shapes were so highly constricted that they could be approximated initially by tangent spheroids. This rather outstanding success can now be understood within the framework of the present results: Fragment-shell effects are relatively weak for this region of compound nuclei, since the fragments are soft midshell nuclei, and furthermore do not appear to change the LDM minimum-potential-energy fission path appreciably. It is reasonable to suppose, therefore, that the fragment-shell effects also do not change the potential-energy surface along coordinate directions orthogonal to the fission direction appreciably. Since it is these coordinates which are dominant in determining the mass and energy distributions, it follows that LDM calculations should be rather successful.

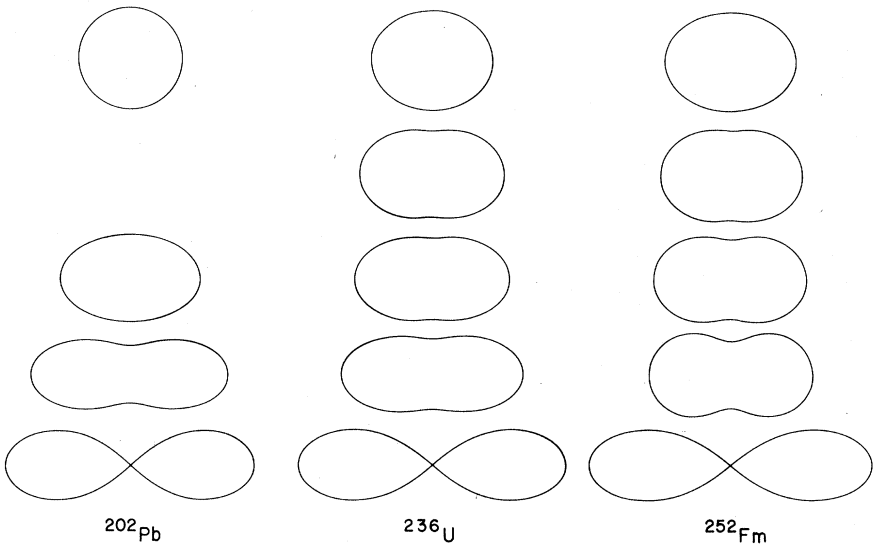

FIG. 12. Nuclear shapes for ^{202}Pb, ^{236}U, and ^{252}Fm at the ground state, the first barrier, the second minimum, the second barrier, and at scission. These shapes correspond to the appropriate points in the shell-corrected potential-energy surfaces.

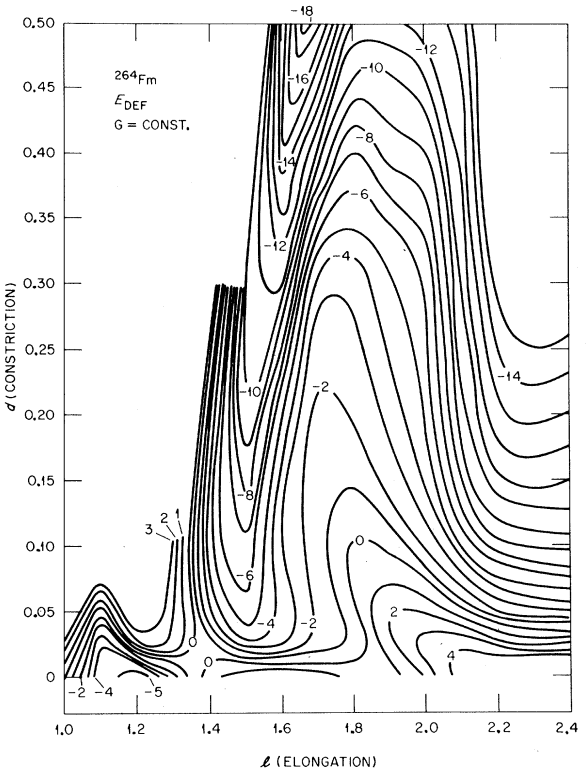

FIG. 13. The PES of ^{264}Fm calculated with a surface-independent pairing strength.

2. $A \gtrsim 230$. In view of our result that fragment-shell effects are important for these nuclei and that their influence extends far into the PES, it is reasonable that the LDM should not be successful in predicting fragment mass and energy distributions. Static scission models,[4,25] however, have been very successful in systematizing fragment kinetic and excitation energies for these nuclei, and even for lighter compound nuclei. The assumption that fragment structure dominates in the latter stages of fission is implicit in such calculations. Our results, based on PES's, substantiate this assumption and render the successes of the static scission models reasonable.[26]

An interesting implication of this consideration may be pointed out; namely, the kinetic energies of fission fragments should be significantly higher for the region of compound nuclei about ^{264}Fm. Here the fragments are formed in the region about $^{132}_{50}Sn_{82}$ and have less elongated shapes. For still heavier nuclei, however, the kinetic energies may again approach the LDM values. Thus a peak at ^{264}Fm is expected when plotting average total fragment kinetic energy as a function of compound-nucleus mass.[26] This prediction is a direct consequence of the strong shell effects of fragment nuclei about $^{132}_{50}Sn_{82}$.

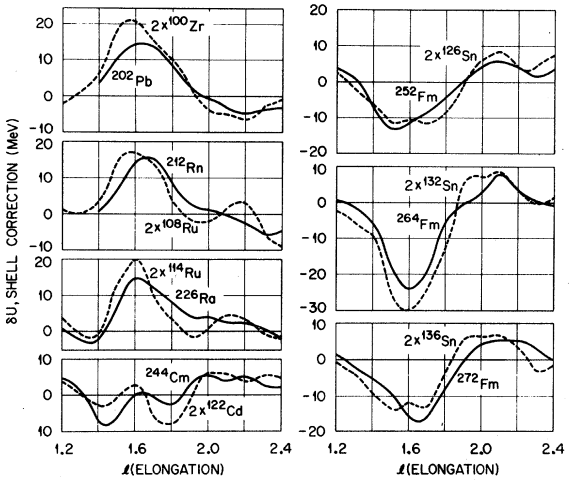

FIG. 14. Shell corrections in the realistic model at $d = 0.5$ as a function of elongation (solid curves) are compared with the total shell corrections for the two independent-fragment nuclei indicated in the figure (dashed curves).

An analysis of the experimental mass distributions shows that through the actinides the mass of the heavier fragment stays almost constant with its distribution peaked at $A \cong 140$.[4] This experimental evidence for fragment influence is again substantiated by the basic results of our calculations showing the dominant influence of the fragment shells throughout most of the fission process. The trend back to symmetry in the mass distribution of ^{257}Fm is thus not too surprising, inasmuch as it reflects an approach to the nucleus ^{264}Fm, where the strong influence of $^{132}_{50}$Sn is again evident. Extrapolating into the superheavy region, it is possible that the mass distributions become asymmetric again, perhaps with the light-fragment peak around mass $A \approx 140$.[26]

Fission isomers. Experiments have shown that the mass and kinetic-energy distributions from the isomeric state are essentially identical to those from the ground state.[27] From our calculations we see that indeed the isomeric states always lie on the static path from the ground state to scission. The experimental results indicate that the fragment mass and energy distributions are determined beyond the second minimum, in agreement with our finding that the fragment shells begin to act immediately after the second minimum in the potential-energy surface.

VIII. ACKNOWLEDGMENTS

One of the authors (U.M.) wishes to thank the Physics Division of Oak Ridge National Laboratory for the hospitality extended to him and to thank especially the members of the fission and theory

groups for their active interest in the calculations reported here. We gratefully acknowledge the help of K. Albrecht and Dr. D. Scharnweber in the early stages of this investigation. Stimulating discussions with Professor W. Greiner are gratefully acknowledged.

---

*Work supported in part by the U. S. Atomic Energy Commission under contract with Union Carbide Corporation.

†Present address: Department of Physics, University of Washington, Seattle, Washington 98105.

[1]M. Bolsterli, E. O. Fiset, and J. R. Nix, in *Proceedings of the Second International Atomic Energy Symposium on Physics and Chemistry of Fission, Vienna, Austria, 1969* (International Atomic Energy Agency, Vienna, Austria, 1969), p. 183; J. R. Nix, private communication; S. G. Nilsson *et al.*, Nucl. Phys. A131, 1 (1969); V. M. Strutinsky and H. C. Pauli, in *Proceedings of the Second International Atomic Energy Symposium on Physics and Chemistry of Fission, Vienna, Austria, 1969* (International Atomic Energy Agency, Vienna, Austria, 1969), p. 155.

[2]V. M. Strutinsky, Nucl. Phys. A95, 420 (1967); A122, 1 (1968).

[3]P. Möller and S. G. Nilsson, Phys. Letters 31B, 283 (1970); H. C. Pauli, T. Ledergerber, and M. Brack, *ibid.* 34B, 264 (1971); V. V. Pashkevich, Nucl. Phys. A171, 275 (1971).

[4]H. W. Schmitt, in *Proceedings of the Second International Atomic Energy Symposium on Physics and Chemistry of Fission, Vienna, Austria, 1969* (International Atomic Energy Agency, Vienna, Austria, 1969), p. 67.

[5]C. Gustafson, P. Möller, and S. G. Nilsson, Phys. Letters 34B, 349 (1971).

[6]P. Holzer, U. Mosel, and W. Greiner, Nucl. Phys. A138, 241 (1969); D. Scharnweber, U. Mosel, and W. Greiner, Phys. Rev. Letters 24, 601 (1970); B. L. Anderson, F. Dickmann, and K. Dietrich, Nucl. Phys. A159, 337 (1970); D. Scharnweber, W. Greiner, and U. Mosel, *ibid.* A164, 257 (1971); C. Y. Wong, Phys. Letters 30B, 61 (1969).

[7]U. Mosel and H. W. Schmitt, Nucl. Phys. A165, 73 (1971); U. Mosel and D. Scharnweber, Phys. Rev. Letters 25, 678 (1970).

[8]J. P. Balagna *et al.*, Phys. Rev. Letters 26, 145 (1971); W. John, E. K. Hulet, R. W. Lougheed, and J. J. Wesolowski, *ibid.* 27, 45 (1971).

[9]S. G. Nilsson, Kgl. Danske Videnskab. Selskab, Mat.-Fys. Medd. 29, No. 16 (1956).

[10]D. A. Arseniev, A. Sobiczewski, and V. G. Soloviev, Nucl. Phys. A139, 269 (1969).

[11]W. D. Myers and W. J. Swiatecki, Arkiv Fysik 36, 343 (1967).

[12]C. Gustafson I. L. Lamm, B. Nilsson, and S. G. Nilsson, Arkiv Fysik 36, 613 (1967).

[13]W. Lin, Phys. Rev. C 2, 871 (1970); J. R. Nix, private communication.

[14]W. D. Myers and W. J. Swiatecki, computer code LYMASS, private communication.

[15]D. S. Burnett *et al.*, Phys. Rev. 134, B952 (1969).

[16]J. R. Huizenga, R. Chaudry, and R. Vandenbosch, Phys. Rev. 126, 210 (1962).

[17]J. R. Nix, and W. J. Swiatecki, Nucl. Phys. 71, 1 (1965); J. R. Nix, *ibid.* A130, 241 (1969).

[18]C. F. Tsang and S. G. Nilsson, Nucl. Phys. A140, 275 (1970).

[19]G. Gneuss, U. Mosel, and W. Greiner, Phys. Letters 30B, 397 (1969); 31B, 269 (1969); 32B, 161 (1970).

[20]S. Bjornholm and V. M. Strutinsky, Nucl. Phys. A136, 1 (1969).

[21]E. Cheifetz, R. C. Jared, S. G. Thompson, and J. B. Wilhelmy, Phys. Rev. Letters 25, 38 (1970).

[22]U. Mosel, J. Maruhn, and W. Greiner, Phys. Letters 34B, 387 (1971).

[23]H. Hofmann and K. Dietrich, Nucl. Phys. A165, 1 (1971).

[24]T. Damgaard *et al.*, in *Proceedings of the Second International Atomic Energy Symposium on Physics and Chemistry of Fission, Vienna, Austria, 1969* (International Atomic Energy Agency, Vienna, Austria, 1969), p. 213; A. Sobiczewski *et al.*, Nucl. Phys. A131, 67 (1967).

[25]H. W. Schmitt, Arkiv Fysik 36, 633 (1967); R. Vandenbosch, Nucl. Phys. 46, 129 (1963); K. Dickmann and K. Dietrich, *ibid.* A129, 241 (1969); see also other references in these papers.

[26]H. W. Schmitt and U. Mosel, to be published.

[27]R. L. Ferguson, F. Plasil, G. D. Alam, and H. W. Schmitt, Nucl. Phys. A172, 33 (1971); Phys. Letters 31B, 526 (1970).